J. Integr. Sci. Technol. 2023, 11(3), 529 Article

Journal of Integrated
SCIENCE & TECHNOLOGY

Investigation of Ru-complex free natural dye for the application of Dye Sensitized Solar Cells

Khushboo Sharma[1], Shyam Sunder Sharma[2*], Jaymin Ray[3], Nandu B. Chaure[4*]

[1]Department of Physics, Bhagwant University, Sikar Road, Ajmer-305004, India. [2]Department of Physics (H & S), Govt. Mahila Engineering College, Ajmer-305002, India. [3]Department of Physics, Uka Tarsadia University, Maliba Campus, Bardoli - 394120, India. [4]Department of Physics, Savitribai Phule Pune University, Pune – 411 007, India

Received on: 02-Dec-2022, Accepted and Published on: 28-Feb-2023

ABSTRACT

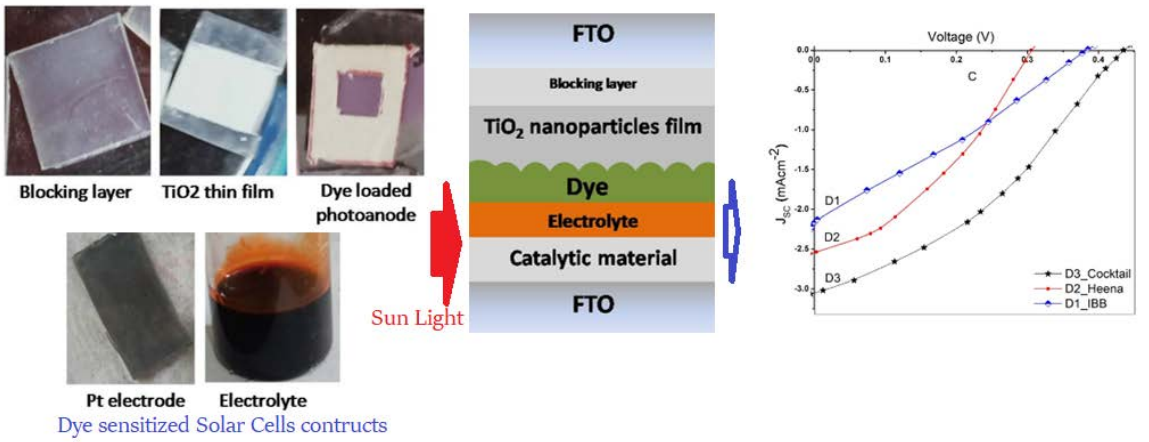

The fabrication and measurement of natural dyes-based Dye sensitized solar cells (DSSCs) have been reported using low-cost solution-processable techniques. Titanium dioxide (TiO_2) nanoparticles have been synthesized by a solvothermal process using Titanium isopropoxide (TIP) as a precursor. Two different natural dyes, Henna (Lawsonia inermis) and Indian blackberry (IBB; Syzgium cumini), and their cocktail were used as natural sensitizers with anatase-based nanostructure of TiO_2 thin film on conducting glass substrate. Scanning electron microscopy (SEM) analysis reveals the uniform distribution of the crystalline anatase phase of TiO_2 upon annealing at 550 ˚C. UV-Vis-NIR spectroscopy and SEM results divulge the absorption capability of dyes and the effect of dye loading on TiO_2 photo-anodes, respectively. Electrochemical impedance spectroscopy (EIS) studies were carried to study the charge transport processes and its effect on the performance of DSSCs. These measurements show the least values of Rpt/Rct and Rpt for D3 dye sensitized DSSC as compare to the other two, with reduced rate of charge recombination resulting from the synergetic effect of co-sensitization of D1 and D2. Thus, the cocktail dye showed promising photovoltaic performance due to an increase in absorption and better dye loading in the device.

Keywords: Solar Cells, Natural sensitizers, TiO_2 nanoparticles, optical spectroscopy, electrochemical impedance spectroscopy

INTRODUCTION

In the modern era of energy conservation, solar cells are playing a very crucial role. Silicon (Si) solar cells cover the major market of high efficient solar cells having a cost-effective approach, because of the well-established production process and ease of raw material availability. In addition to Si, chalcopyrite and perovskite[1] technology had also shown the capability in the cost-effective renewable energy generation. Besides the performance and capability of commercialized solar cells, the high fabrication cost and raw material cost remarkably hinder the affordability to everyone.[2] Comparatively, Dye-sensitized solar cells (DSSCs) demonstrate persuasive as the better solar cells because of the cost-effective raw material, ease, and simple fabrication process. In addition to that, its environmental friendly characteristic gives these solar cells the utmost priority under today's hazardous environment challenges.[3–5]

The very first DSSC was co-invented by Brian O'Regan and Michael Grätzel at UC Berkeley, in 1988.[6] Afterward, various

*Corresponding Author: Dr. S.S. Sharama, Dr. N. B. Chaure
Email: shyam@gweca.ac.in (SSS); n.chaure@physics.unipune.ac.in (NBC)

Cite as: *J. Integr. Sci. Technol., 2023, 11(3), 529. URN:NBN:sciencein.jist.2023.v11.529*

 ISSN: 2321-4635
http://pubs.thesciencein.org/jist

studies reflected that the stability issue is the major challenge to make DSSCs commercialized, where Ru-complex-based dyes played a major role in terms of cells efficiency and performance. However, Ru-complex-based dyes have certain limitations like their cost, scarcity in the availability of the bare material, toxicity, and hence these are unfriendly to the environment.[7] Thus, researchers have carried out several experiments to replace the Ru complex-based sensitizers with metal-free-organic dyes,[8] natural dyes[9,10] and organic complexes of other metals.[11]

Specifically, if one focuses on the natural dyes containing anthocyanin, chlorophyll, and flavonoid as a building material,[10] the natural dye-sensitized solar cells (NDSSCs) show moderate performance compared to the other sensitizers based DSSCs.[12] Nevertheless, the obtrusive advantage of natural dye is its easy and wide availability and cost-effective processing. This makes it desirable for next-generation solar photovoltaic, upon further performance encroachment. Various fruits, flowers, and vegetable extract-based natural sensitizers have shown effectiveness in the energy generation process through DSSCs.[9,13] The finest performance of the natural dyes-based DSSCs shows about 1% power conversion efficiency (PCE), respectively. However, the blend of the natural dyes was not explored much and a lack of detailed study on the properties of these natural sensitizers has been provided, specifically in terms of impedance, dielectric, and FTIR analysis.

In the present study, Indian blackberry (IBB), henna, and their cocktail were used as sensitizers for the fabrication of DSSCs. Annealed porous TiO_2 (act as a photo-anode) was used to fabricate the DSSCs and characterized by scanning electron microscopy (SEM), electrochemical impedance spectroscopy (EIS) measurement, and current-voltage (I-V) measurement. SEM includes the topography analysis and cross-section analysis of the prepared DSSCs. EIS and J-V curve explores the process for the utilization of generated charges.

EXPERIMENTAL

Materials

Analytical grade of Titanium Isopropoxide (TIP), Acetic Acid (AA), and Ethanol were purchased from Sigma-Aldrich and were used without any purification for the synthesis of TiO_2. Ethylene cellulose (EC), α-Terpineol, and acetylacetone were purchased from Merck chemicals and used for the preparation of the TiO_2 paste. Potassium iodide was purchased from Loba chemicals.

Synthesis

Synthesis of TiO_2 by solvothermal process

The solvothermal process was used to synthesize pure and homogeneous TiO_2 NPs.[14,15] Solution A was prepared by adding 50 ml of ethanol into 0.014 M of AA under continuous stirring. After 45 min. of stirring, 0.14 M of TIP was added into solution A dropwise. The prepared solution was kept under continuous stirring for about 30 minutes. Finally, the solution was autoclaved at 180 ºC for 18 hours and left as it is until naturally cools down at room temperature (RT). The as-synthesized TiO_2 was centrifuged at 12000 rpm and washed thrice with ethanol to remove any remained contamination or the byproducts. The resultant suspension was dried under IR lamp and calcinated at 550 ºC in a furnace (optics technology) for 18 hours to obtain highly crystalline particles, which is generally required for reduced electron and hole recombination at defective site hence improved light absorption.

Synthesis of Natural Sensitizers

For the synthesis of Indian blackberry (IBB) and henna as a dye, the IBBs were washed with distilled water and ethanol several times to remove any dirt or pesticides. Subsequently, the IBB's were crushed and left in ethanol overnight and the juice was filtered with filter paper and used as dye D1. The henna paste was purchased from the nearby local market and used as a sensitizer by diluting it in ethanol; as D2 dye. The third sensitizer, D3 dye, was prepared by making a cocktail of both dyes i.e., mixing dye D1 and D2 in the same volume ratio. The chemical structures of both IBB and henna were shown in Figure 1.

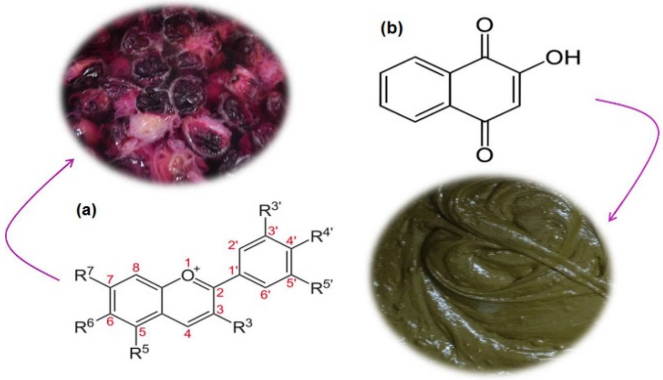

Figure 1: Chemical Structure of (a) Anthocyanin and (b) Lawsone, the key component responsible for the color in IBB and henna plants, respectively.

Fabrication of Photo-anode

TiO_2 paste was prepared by crushing 1 g of TiO_2 in a mortal pestle with ethanol to achieve the finest granular form. 0.7 g of crushed ethylene cellulose (EC) and 2 g of α-Terpineol was added to the TiO_2 and sonicated for almost 3 hours. Finally, a few drops of acetylacetone were added to the above paste. A blocking layer of TiO_2 was coated onto Fluorine Doped Tin Oxide (FTO) coated glass substrate (blocking layer/FTO coated film ~400 nm) by spin coating technique. This blocking layer works as a barrier towards any direct contact between the FTO, the sensitizer, and an electrolyte resulting in a deceased hole-electron recombination process and improved dye loading. The blocking layer was obtained by diluting a small amount of TiO_2 paste in ethanol by spin coating the solution over FTO at 1000 rpm for 30 s following further spinning of 4000 rpm for 30 s. Finally, as-prepared TiO_2 paste was coated (~8 µm) onto blocking layer/FTO plates using Doctor Blade technique and kept for sintering at 450 °C for an hour. Finally, the photo-anodes were soaked within different sensitizers as D1 (IBB), D2 (henna), and D3 (cocktail) for 20 hours, and washed with ethanol twice to restrain any dye agglomeration over photo-anode surface.

Fabrication of Counter Electrode

A solution of Chloroplatinic acid (50 mg) in 15 ml of ethanol was prepared for the deposition of platinum (Pt) onto the FTO glass

substrate. Further, the as-prepared H2PtCL6 solution was deposited over the FTO for 15-20 min using a water bath, whose temperature was maintained at 90 °C constantly. Afterward, the prepared Pt counter electrode was sintered at 450 °C for 30 minutes to secure the film.

Assembling of DSSCs

To complete the cell assembly, a few drops of potassium iodide electrolyte (0.1 M of KI, 0.05 M of I2, 0.6 M of 1,2-dimethyl-3-n-propylimidazoliumiodide (DMPII) and 0.5 M of 4-tertbutylpyridine (TBP) in acetonitrile) were inserted in between both TiO_2 photo-anode and Pt counter electrode. The entire cell was secured with the help of binder clips. The final active surface area of DSSCs was taken as 0.5 cm2 via a spacer. The basic sandwich structure and relative components of dye-sensitized solar cells with a laboratory sample are shown in Figure 2.

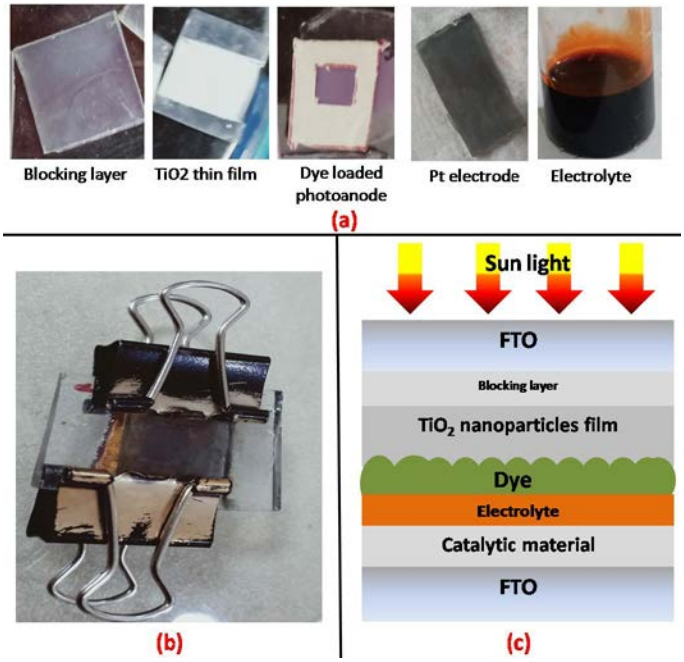

Figure 2: Schematic showing (a) basic components of a DSSC; (b) laboratory sample cell; and (c) sandwich structure of DSSCs, respectively.

Characterizations

The current density–voltage (J-V) measurements of the devices were carried out on a computer-controlled Keithley electrometer 2450 under illumination with power intensity 100 mWcm-2. UV-Vis-NIR spectra were recorded on UV-1800 Shimadzu spectrophotometer in the range of 300 nm to 800 nm and the XRD was recorded from 20° to 80° using Brucker D8, Advanced Diffractometer instrument, having CuKα anode with λ = 1.5406 Å. Jasco FTIR-6100 spectrometer was used to study the molecular properties of the samples. The topographical images of different photo-anodes were recorded using a JEOL JSM-6360A scanning electron microscope at 20 kV with secondary electron imaging (SEI) and backscattered electron imaging (BEI) and 6000 times of photo-magnification. Electrochemical impedance spectroscopy (EIS) measurements for DSSCs were performed using a Biologic SP300 potentiostat under illumination and an AC signal of 10 mV with a frequency between 50 to 200 Hz.

Results and Discussion

Structural properties

X-ray Diffraction Microscopy (XRD)

XRD measurements were employed to examine the structural properties and average crystallite size of the as-synthesized TiO_2 nanoparticles, in addition to evaluate the purity. Figure 3 (a) and 3 (b) show the XRD profiles of as-prepared and annealed TiO_2 at 550 °C, respectively. Figure 3 (a) represents the XRD pattern of the as-prepared titania, portrayed with the peaks at 2θ = 25.27º, 37.88º, 48.14º, 53.99º, 55.16º, 62.78º, 68.8º, 70.41º, and 75.17º, which are respectively identified to (101), (004), (200), (105), (211), (204), (116), (220) and (215) Bragg reflections, attributed to the anatase phase of crystalline TiO_2. Similarly, Figure 3 (b) represents the XRD patterns of annealed TiO_2 with all the observed miller planes of pristine sample along with additional planes as (103), (112) and (301) at 2θ of around 37.03º, 38.66º and 76.11º,[14] which also confirms anatase phase of crystalline TiO_2. The anatase phase of TiO_2 is considered to be more preferable than rutile for the fabrication of DSSCs because of greater per-unit active sides, and hence higher photoactive ability.[16] Also, the sharp-intense peaks exhibited by the calcinated TiO_2 NPs can be clearly seen from the XRD pattern that shows a higher crystallinity of the as-synthesized TiO_2 NPs[17] and embraces its potent application in DSSCs with a high efficacy.

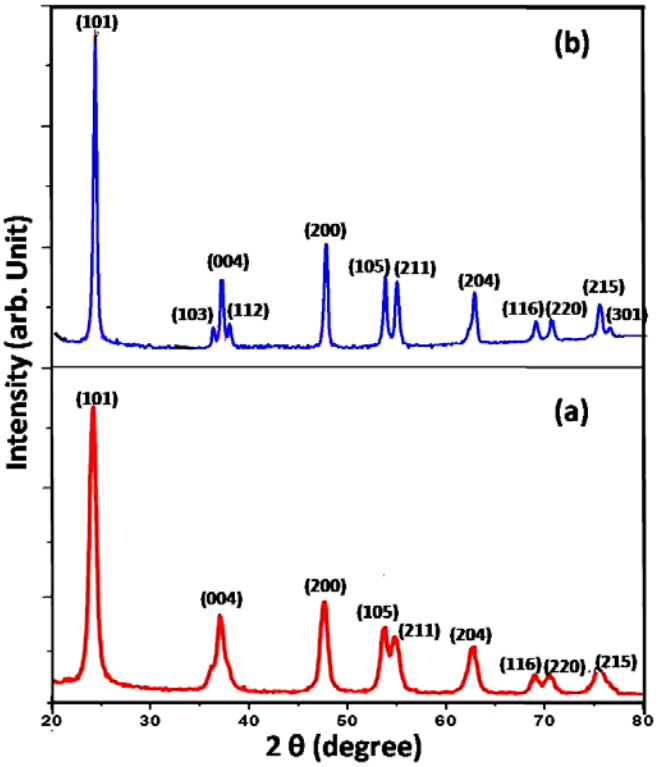

Figure 3: Representative XRD patterns for (a) pristine and (b) calcinated (at 550 °C) TiO_2 nanoparticles.

The Debye Scherrer's equation was used to calculate the average crystallite size (D in nm) of the as-synthesized TiO_2 NPs,[18]

$$D = \frac{K\lambda}{\beta \cos\theta} \quad (1)$$

where, K is the Scherrer constant taken to be, 0.9 considering the spherical shapes of particle, λ is the wavelength of the X-ray sources (1.5406 Å); β is the Full width at half maxima (radians); and θ is the peak position (radians), respectively. Table 1 encapsulates the value of the average crystallite size of raw as well as calcinated TiO_2 NPs, respectively.

Table 1: The structural parameters (evaluated from XRD) of the as prepared and calcinated TiO_2 (at 550 °C).

2θ (°)	Miller Planes	FWHM (radians)	Average Crystallite Size (nm)	Crystallite Size (nm)
Pristine TiO_2				
25.27	(101)	0.4251	20 ± 0.2	~ 22
37.88	(004)	0.3503	25 ± 0.4	
48.14	(200)	0.3758	24 ± 0.2	
53.99	(105)	0.3783	24 ± 0.5	
55.16	(211)	0.3739	25 ± 0.6	
62.78	(204)	0.4984	19 ± 0.7	
68.80	(116)	0.4851	20 ± 0.8	
70.41	(220)	0.5102	19 ± 0.7	
75.17	(215)	0.4577	22 ± 0.4	
Calcinated TiO_2				
25.41	(101)	0.3440	24 ± 0.1	~ 26
37.03	(103)	0.3006	29 ± 0.4	
37.83	(004)	0.2699	32 ± 0.3	
38.66	(112)	0.3117	28 ± 0.5	
48.15	(200)	0.3217	28 ± 0.2	
53.96	(105)	0.3453	26 ± 0.2	
55.17	(211)	0.3787	24 ± 0.2	
62.78	(204)	0.4837	20 ± 0.3	
68.79	(116)	0.4120	24 ± 0.5	
70.30	(220)	0.3882	26 ± 0.6	
75.11	(215)	0.4147	25 ± 0.2	
76.11	(301)	0.4718	22 ± 0.6	

The estimated crystallite size for the as-synthesized TiO_2 NPs observed from the XRD peaks is in the range of nano dimension, i.e. ~ 22 nm, which further increases up to ~ 26 nm upon calcination. This improved crystalline size indicates a reduction of surface defects of materials that leads to the proper growth of particles and the nucleation rate.[19]

Scanning Electron Microscopy (SEM)

Figure 4 shows the SEM images of un-sensitized and sensitized TiO_2 photo-anodes. Figure 4 (a) demonstrates an un-sensitized TiO_2 photo-anode, whereas Figure 4 (b-d) shows TiO_2 photo-anodes sensitized with D1, D2, and D3 dyes, respectively. To estimate the thickness of the TiO_2 films coated on the blocking layer/FTO substrate, the cross-section morphology is shown as Figure 4 (e). Also, the cross-section SEM elaborates the better adhesion between FTO glass plate, blocking layer, and the TiO_2 layer. In addition to that, the better porosity (due to uniform grains) of the TiO_2 layer (~ 8 μm) attained upon annealing the photo-anode at 450 ˚C can be clearly seen in Figure 4 (a) and (e) along with smooth and crack-free appearance on the surface which is a desirable and suitable parameter for higher dye loading and reduced recombination rate of carriers, resulting in higher JSC values of DSSCs.[13] This higher nanocrystallinity and nanoporous structure composed of interconnected NPs observed for the TiO_2 layer results in a higher roughness factor thus ensuring larger staining of the dye molecules, and deeper penetration of electrolyte into the film,[20] resulting in an efficient dye/TiO_2/electrolyte interface. The thickness of TiO_2 films also play a crucial role in the performance of the DSSCs as increase of the thickness of TiO_2 give rise to increase in grain size that simultaneously effects the efficacy of the DSSCs.[21] Thus, TiO_2 film with an average thickness of ~ 8-9 μm is coated over blocking layer/FTO glass plates of thickness ~0.4 μm. Further, more uniformity and fewer cracks in the film is visible for the sensitized TiO_2 photo-anodes in the order D1 < D2 < D3 upon dye loading as illustrated in Figure 4 (b-d). The more smoother and uniform film surface for the cocktail sensitized TiO_2 photo-anode implies the higher dye loading with minimum agglomeration in D3 sensitized TiO_2 photo-anode, which may be attributed to the blend of dye D1 and D2 resulting in maximum grain sites occupation of TiO_2 through the cocktail of D1 and D2 dyes and their molecules.[22] This results in higher incident photon absorption by the molecules of cocktail dye over TiO_2 nanoporous photo-anode. Thus, higher dye loading in D3 based devices improves the performance of NDSSCs

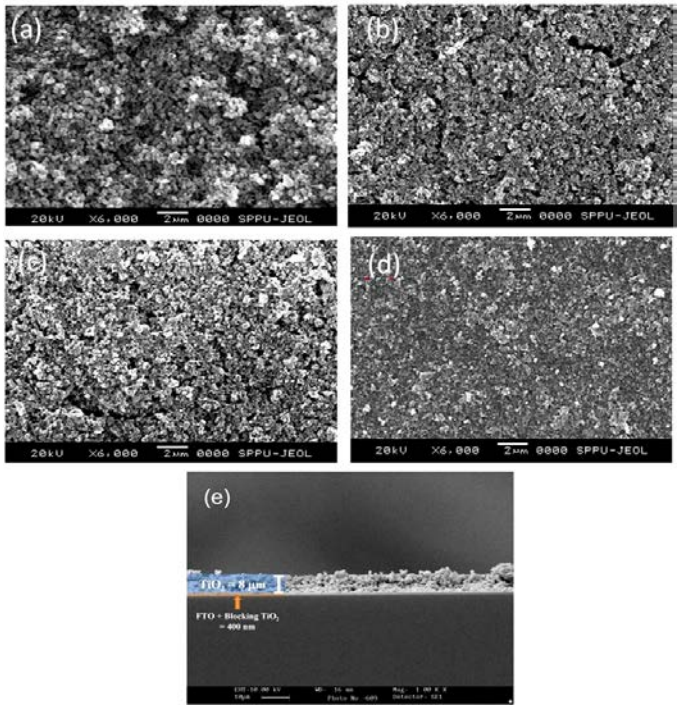

Figure 4: SEM images of (a) un-sensitized TiO_2 photo-anode; TiO_2 photo-anodes sensitized with dye (b) D1, (c) D2, and (d) D3; and (e) cross-section morphology of TiO_2 photo-anode, respectively.

by providing more electrons towards external circuit via TiO_2/FTO. Therefore, it may conclude that more is the porosity of the semiconducting oxide film higher will be the dye loading, triggering efficient electron-hole regeneration and better PV performance of the DSSCs.

Optical Properties

The optical absorption spectra of TiO_2 photo-anodes sensitized with extracted natural dyes and their cocktail were measured at room temperature in the wavelength range of 300 nm to 800 nm. As shown in Figure 5, absorption spectrum for all three photo-anodes falls between 340 nm to 800 nm. The sharp absorption edge below 340 nm (region (I)) signifies the absorption due to the TiO_2. The absorbance peaks (both weak and strong) are exhibited for all three dyes at 338 nm, 385 nm, 465 nm, and 540 nm, respectively. The absorption peak at 385 nm wavelength signifies the attachment of hydroxyl-functional group (OH) at the benzene ring in henna.[23] Peak at 334 nm corresponding to n-π* transition, and absorbance band around 457 nm may be associated with the π- π* transitions of the carbonyl group in the quinone ring.[24,25] The absorption characteristics of IBB dye are well supported by earlier reports where a small change in slope is seen between 370 nm - 415 nm.[26] An absorption shoulder around 338 nm is visible for n-π* transitions for D1 sensitized TiO_2 photo-anode.[27] It depicted that the surface amino group leads a broad transition around 340 nm – 400 nm with the shoulder at 338 nm. The result reveals the capability of all three dyes as sensitizers in DSSCs. Thus, the light absorbance observed for all three dyes is appreciable which resulted in a higher value to JSC. Further, it can be seen in Figure 5 (c), the absorption peaks are slightly more intense and broad for D3 dye indicating maximum photon absorption in case of cocktail dye as compared to individual dye photon absorption, resulting in better device performance for DSSCs applying D3 dye as a sensitizer.

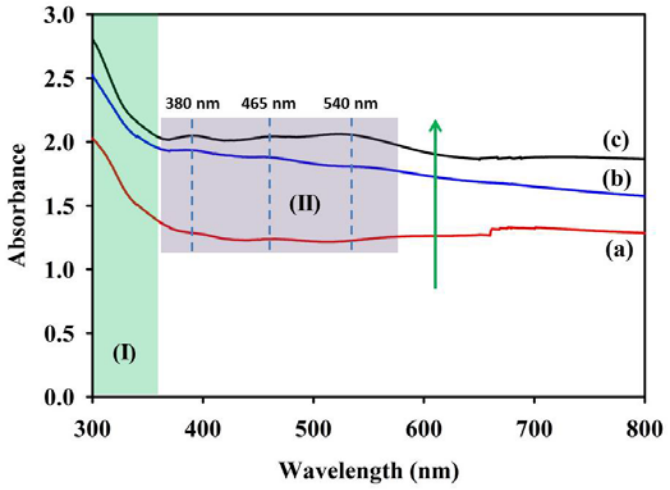

Figure 5: UV-Vis absorbance of photo-anodes sensitized with (a) D1, (b) D2, and (c) D3 dyes.

Fourier Transform Infra-Red (FTIR) spectroscopy

FTIR spectroscopy was employed to identify the bond's functional groups present in the prepared dyes. The sample was kept over the germanium crystal and infrared radiations were passed through the sample. The presence of two major frequency regions of the band, i.e., hydroxyl (OH) and carbonyl (C=O) group have been shown in the FTIR spectrum as Figure 6, where lawsone (2-hydrox, 1, 4-naphthoquinone; HNQ) is represented by the hydroxyl group,[23] as the hydroxyl groups on the surface of TiO_2 film improves the dye concentration in the film which plays a vital role in the performance of the cell.[28] Broadband at 3340 cm-1 shows the stretching vibration of the OH group present at the first lawsone aromatic ring.[29,30] This broad absorption band was due to the intramolecular hydrogen bonding between the hydroxyl group and adjacent oxygen atom.

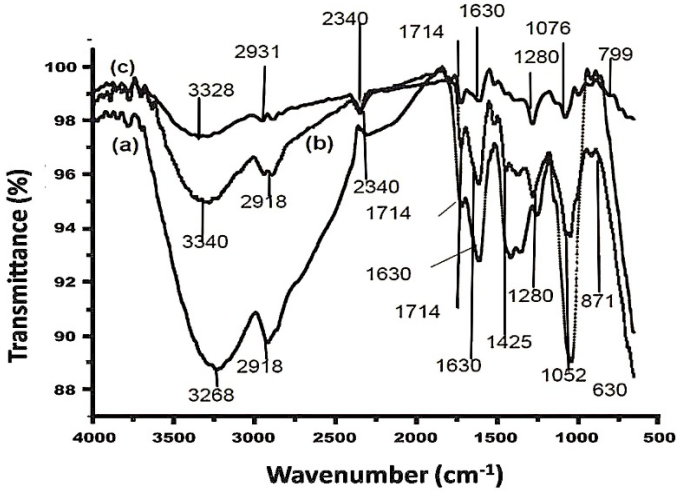

Figure 6: FTIR spectra of different dyes as (a) D1, (b) D2, and (c) D3.

The carbonyl band of quinones falls in the frequency range of 1655 – 1690 cm-1 (Brown 1962). The α-β-unsaturated carbonyl bands and C=C group were revealed at 1714 and 1630 cm-1 absorption bands.[31] A weak absorption band at 1425 cm-1 was signified by the aromatic C=C group. In the case of D1 sensitizer, a broad absorption band was observed at 3268 cm-1 for the hydroxyl group with stretching vibration, where 3429 cm-1 is the standard value for anthocyanin.[32] At frequency 2918 cm-1 the stretching aliphatic hydrogen bond and weak absorption band at 1714 cm-1 were accredited to the carbonyl group. C=C of benzene ring was signified at 1630 cm-1 as shown in Figure 6. In the IR spectra of the cocktail, the absorption bands are found to be shifted from 3268 cm-1 to 3328 cm-1 with a much broader absorption band for the OH group at 3328 cm-1 indicating the presence of many different bonding states of OH groups may be attributing higher efficiency for D3 sensitized DSSC. Thus, FTIR data have proven the presence of important carbonyl and hydroxyl group in the prepared natural dyes, which binds with the TiO_2 readily as capable of chelating with Ti (IV) sites on the TiO_2 surface and supports the electron generation process.[33] Table 2 summarizes the identification of absorption bands present in the as-prepared photosensitizers D1, D2, and D3.

Table 2: IR spectrum table by frequency range for different as-prepared photosensitizers

Photosensitizer	Absorption (cm^{-1})	Group	Appearance
D1	3268	OH stretching	Strong
	2918	C-H stretching	Sharp
	1714	C=O stretching	Weak
	1630	C=C stretching	Strong
	1052	C-O stretching	Sharp
D2	3340	OH stretching	Broad
	2918	C-H stretching	Medium
	2340	O=C=O stretching	Sharp
	1714	C=O stretching	Sharp
	1630	C=C stretching	Strong
	1425	C=C stretching	Weak
	1280	C-O stretching	Strong
	1052	C-O stretching	Sharp
D3	3328	OH stretching	Broad
	2931	C-H stretching	Weak
	2340	O=C=O stretching	Sharp
	1714	C=O stretching	Weak
	1630	C=C stretching	Broad
	1280	C-O stretching	Sharp
	1076	C-O stretching	Medium

Photovoltaic Properties

Current Density-Voltage (J-V) Characteristic

The photovoltaic parameters of all three devices based on different natural photosensitizers D1, D2, and D3, are shown as Table 3. The fabricated cells were illuminated under (AM1.5), 100 $mWcm^{-2}$ at maintained 25 °C ambient temperature. The PV performance of all three DSSCs based on dyes D1, D2, and D3 is shown as Figure 7. An improved value of VOC as well as JSC along with higher conversion efficiencies were exhibited by D3 based DSSCs. Noticeable improvement in JSC observed for D3 based device directs their potent of generating dense electron distribution at the TiO_2 surface and thus, an effective ejection of electron through photo-electrode to external circuit.[34] Also, an overall increase of ~ 112.5 % and 75.8 % in efficiency was observed for D3 based device then the DSSCs based on individual dyes D1 and D2, which was further explained via charge transport dynamics in these devices, where, the values of resistance, Rct and RPt, for all three devices are calculated through EIS spectroscopy.

Table 3: PV performance of all three devices based on D1, D2, and D3 photosensitizers.

Device	J_{SC} (mA cm^{-2})	V_{OC} (V)	*FF* (%)	η (%)	R_{ct} (kΩ)	R_{Pt} (kΩ)
D1	2.15	0.38	29	0.24	160	30
D2	2.54	0.30	38	0.29	58	29
D3	3.05	0.44	38	0.51	25	16

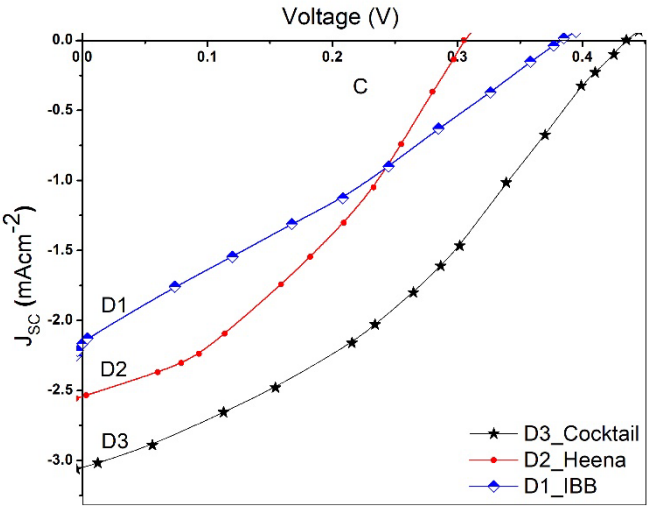

Figure 7: J-V characteristics of all the three devices based on D1, D2, and D3 photosensitizers.

The better PV performance for D3 based DSSC is well supported with the optical properties and morphological study of D3 sensitized photo-anode along with the IR studies. Thus, the better cell performance of D3 based device may attribute to its higher dye adsorption onto TiO_2 surface resulting in improved values of JSC and VOC due to more electron-hole pair generation. This improves the dye/TiO_2/electrolyte interface resulting in faster dye oxidation through electrolyte thus amplifying the JSC of the cell.

Lower JSC and VOC values for individual D1 and D2 based devices as compared to D3 based cell, indicates the less efficient dye adsorption of D2 and D3 at TiO_2 surface, effecting the transfer of electrons from LUMO (lowest unoccupied molecular orbital) to Fermi level of the semiconducting oxide layer.[35] In case of D1 based device, lower values of JSC may be accredited to their molecular structure as anthocyanin concentration in Jamun (<2.5 mg/gram) is significantly lower thus ascribing lower photon adsorption at the TiO_2 surface.[36] Also, a weaker dye adsorption at the TiO_2 surface reflects weaker photo-anode/electrolyte interface,

thus, triggering higher charge recombination at the dye/photo-anode/electrolyte interface resulting in poor PV performance of the devices D1 and D2. Also, the reduction of VOC in D2 based device may attribute to the increased surface area and the positively shift of conduction band edge (Fermi level) of TiO_2. However, this positive shift with respect to dye energy levels narrows the energy difference between TiO_2 and dye, assisting photosensitizer to inject more electrons resulting in enhanced JSC in D2 based DSSC.[37] Thus, the J-V characteristics of fabricated DSSCs are well supported by the different characterizations. However, the efficiency can be further improved by optimizing the solvent use to prepare dye, thickness of the TiO_2 layer, and varying dye-loading time etc. because the optimized combinations of all these factors show a huge impact on the efficacy of the DSSCs.[21,22,38]

Electrochemical impedance spectroscopy (EIS)

The photogenerated electron transport mechanism can be evaluated through EIS spectra studies, by applying a small amount of alternating voltage to prepared DSSCs. It gives the specific voltage and current values at a specific angular frequency. By using these values, impedances of the fabricated DSSCs were plotted, which are generally known as a Nyquist plot or Bode plot. Depending on the values of the impedance one can derive the important parameters related to the electron transfer phenomena, such as electron transport through porous TiO_2 film, TiO_2/electrolyte interface recombination, charge transfer near and at the counter electrode, etc. Figure 8 shows the illuminated EIS plot, i.e. Nyquist plot of the prepared DSSCs comprising of semicircles shape of the impedance spectra.

All three spectra consist of one small and one large semi-circle that represents the charge transfer resistance at the counter electrode/electrolyte interface (Rpt) and charges transfer resistance due to the charge recombination process between electrons in the tri-iodide in the electrolyte and TiO_2 film (Rct) respectively. The values of RPt for the cells D1, D2, and D3 are 30 kΩ, 29 kΩ and 16 kΩ respectively (Figure 8 (ii)). While the values for Rct for the cells D1, D2, and D3 are 160 kΩ, 58 kΩ, and 25 kΩ respectively (Figure 8 (i)).

The high values of Rct generally represent the weaker binding of the extract to TiO_2 or the aggregation of the extract on the TiO_2 porous structure.[39,40] These certainly influence the photovoltaic performance of the DSSCs by restricting the efficient injection of electrons from LUMO of dye to CB of TiO_2 layer thus increasing the rate of charge recombination at dye/photo-anode/electrolyte interface. As illustrated in Table 3 and shown in Figure 7, DSSC with D3 dye shows the least Rct values as compare to the other two Devices based on dyes D1 and D2, resulting from the synergetic effect of co-sensitization of dye D1 and D2. A reduced value of Rct in the order D3 < D2 < D1 indicates good charge transfer kinetics and strong dye anchoring on highly porous TiO_2 film, limiting the charge recombination process and greater dye adsorption in D3 based DSSC.[41]

On the other hand, RPt represents the charge transfer resistance at the Pt/electrolyte interface. The smaller values of RPt are always desirable in the case of DSSCs that allows faster electron transfer diffusion that leads to improve the performance of the cell. In the presented results, the cell shows the best performance when the RPt

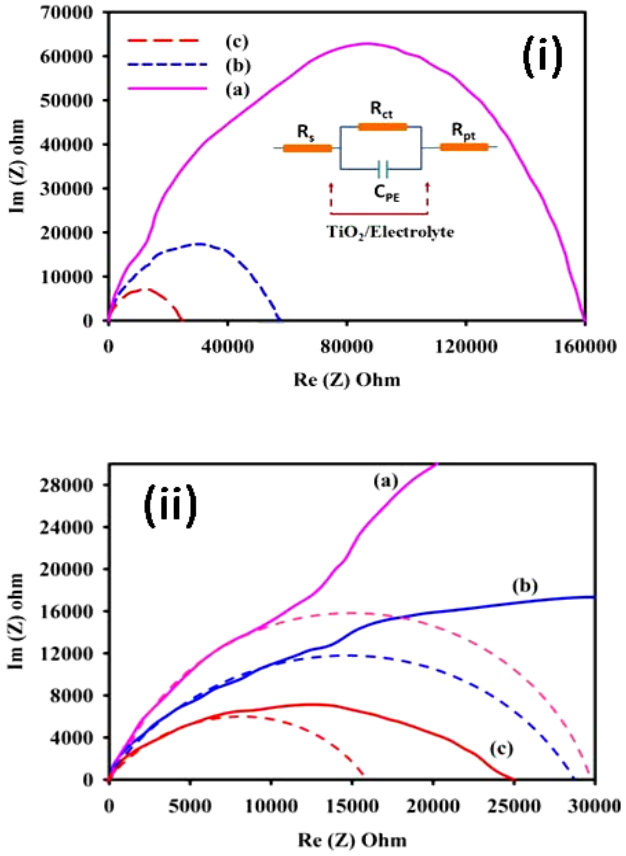

Figure 8: EIS plot of fabricated DSSCs (i) full spectra (inset shows the equivalent circuit) and (ii) closer view of spectra at higher frequencies. Whereas (a) indicates D1 based device; (b) indicates D2 based device; and (c) indicates D3 based device.

values are minimum i.e. 16 kΩ for D3 based devices directing fast electron transport at Pt/electrolyte interface in D3 based DSSCs ensuing faster I3- oxidation process.[42,43] Again, the RPt values are lower than the Rct values for all three dyes, where, Rpt/Rct value for D3 cockatil dye is slightly higher than 1 which is also minimum as compared to other individual dyes, D1 and D2.[34] Concisely, high values of both parameters certainly influence the cell performance that may lead to the lower fill factor of all prepared DSSCs.

CONCLUSION

TiO_2 NPs have been synthesized through a low-cost solvothermal process and further used to prepare the photo-anode for DSSCs based on naturally sensitized IBB, henna, and their cocktail. XRD results confirmed the synthesis of anatase TiO_2 nanoparticles with an average crystallite size of 26 nm upon annealing at 550 ˚C. The natural sensitizers IBB and henna have been chosen due to the presence of hydroxyl group in the selected dyes as confirmed by the FTIR spectroscopy. The DSSCs based on cocktail dye showed highest device performance with η = 0.51 %, VOC = 0.44 V and JSC = 3.05 mAcm-2. This is due to the increased photon absorption range from 340 nm to 640 nm and a more uniform surface for photo-anode sensitized with cocktail dye due to higher dye loading. EIS study elaborates the lowest charge transfer

resistance at the counter electrode/electrolyte interface that enhanced the performance of cocktail dye-based DSSCs. Thus, cocktail dye is found as an effective way to enhance the efficiency of the device.

ACKNOWLEDGEMENT

The authors would like to acknowledge the Department of Science & Technology, SERB Division, Govt. of India, for providing experimental facilities developed under the sanctioned project (Award#SR/FTP/PS-112/2012 Dated 1.11.2013) and Material Science lab developed at GWEC, Ajmer under TEQIP-II.

CONFLICT OF INTEREST STATEMENT

The authors declare that they have no known competing financial interests or personal relationships that could have appeared to influence the work reported in this paper.

AUTHORS' CONTRIBUTIONS

All authors contributed to the study, conception and design. The work plan was designed by Khushboo Sharma and Shyam Sunder Sharma. Materials preparation, data collection and analysis were performed by Khushboo Sharma and Jaymin Ray. The first draft of the manuscript was co-written by Khushboo Sharma and Shyam Sunder Sharma, and Nandu B Chaure and Jaymin Ray commented on previous versions of the manuscript. All authors read and approved the final manuscript, finally developed the concept.

REFERENCES AND NOTES

1. C.V. Rudrappa, S. Ganesan. Investigation of performance and stability of multilayered organometallic halide Perovskite cell. *J. Integr. Sci. Technol.* **2023**, 11 (1), 465.
2. S. Mathew, A. Yella, P. Gao, et al. Dye-sensitized solar cells with 13% efficiency achieved through the molecular engineering of porphyrin sensitizers. *Nat. Chem.* **2014**, 6 (3), 242–247.
3. M. Grätzel. Dye-sensitized solar cells. *J. Photochem. Photobiol. C Photochem. Rev.* **2003**, 4 (2), 145–153.
4. T.V.B. Nagaveni, K.M. Mahadevan, R. Naik, T.O.S. Kumara. Synthesis of blue light emitting 5-carboxylicacid-2-arylsubstituted benzimidazoles as photosensitizers for dye-sensitized solar cells. *J. Mater. Nanosci.* **2020**, 7 (1), 24–28.
5. B. Siwach, S. Sharma, Mohan, D. Structural, optical and morphological properties of ZnO/MWCNTs nanocomposite photoanodes for Dye Sensitized Solar Cells (DSSCs) application. *J. Integr. Sci. Technol.* **2017**, 5 (1), 1–4.
6. B. O'Regan, M. Grätzel. A low-cost, high-efficiency solar cell based on dye-sensitized colloidal TiO2 films. *Nature*. 1991, pp 737–740.
7. K. Sharma, V. Sharma, S.S. Sharma. Dye-Sensitized Solar Cells: Fundamentals and Current Status. *Nanoscale Res. Lett.* **2018**, 13, 381.
8. S.E. Mahmoud, A.A. Fadda, E. Abdel-Latif, M.R. Elmorsy. Synthesis of Novel Triphenylamine-Based Organic Dyes with Dual Anchors for Efficient Dye-Sensitized Solar Cells. *Nanoscale Res. Lett.* **2022**, 17 (1), 71.
9. R.E.Y. Adu, G. Gelyaman, M.M. Kollo, M.A. Talan. Dye-Sensitized Solar Cell (DSSC) Fabrication Using Methanol Extract of Onion Peel as a Natural Sensitizer. *J. Turkish Chem. Soc. Sect. A Chem.* **2022**, 9 (4), 1285–1294.
10. S. Sunder Sharma, K. Sharma, R. Singh, et al. Natural pigments: Origin and applications in dye sensitized solar cells. *Mater. Today Proc.* **2021**, 42, 1744–1748.
11. E.A.M. Geary, L.J. Yellowlees, L.A. Jack, et al. Synthesis, structure, and properties of [Pt(II)(diimine)(dithiolate)] dyes with 3,3′-, 4,4′-, and 5,5′-disubstituted bipyridyl: Applications in dye-sensitized solar cells. *Inorg. Chem.* **2005**, 44 (2), 242–250.
12. S. Sardar, P. Kar, S.K. Pal. The Impact of Central Metal Ions in Porphyrin Functionalized ZnO/TiO2 for Enhanced Solar Energy Conversion. *J. Mater. Nanosci.* **2014**, 1 (1), 12–30.
13. N. Sawhney, A. Raghav, S. Satapathi. Utilization of Naturally Occurring Dyes as Sensitizers in Dye Sensitized Solar Cells. *IEEE J. Photovoltaics* **2017**, 7 (2), 539–544.
14. D. Dastan, N. Chaure, M. Kartha. Surfactants assisted solvothermal derived titania nanoparticles: synthesis and simulation. *J. Mater. Sci. Mater. Electron.* **2017**, 28 (11), 7784–7796.
15. M. V. Bhute, Y.P. Mahant, S.B. Kondawar. Titanium dioxide / poly(vinylidene fluoride) hybrid polymer composite nanofibers as potential separator for lithium ion battery. *J. Mater. Nanosci.* **2017**, 4 (1), 6–12.
16. D.O. Scanlon, C.W. Dunnill, J. Buckeridge, et al. Band alignment of rutile and anatase TiO2. *Nat. Mater.* **2013**, 12 (9), 798–801.
17. R. Subodro, B. Kristiawan, A.H. Ramelan, et al. Dye-Sensitized Solar Cells (DSSCs) reengineering using TiO2 with natural dye (anthocyanin). *AIP Conf. Proc.* **2017**, 1788, 30104.
18. M. Sundrarajan, K. Bama, M. Bhavani, et al. Obtaining titanium dioxide nanoparticles with spherical shape and antimicrobial properties using M. citrifolia leaves extract by hydrothermal method. *J. Photochem. Photobiol. B Biol.* **2017**, 171, 117–124.
19. S. Mahshid, M. Askari, M. Sasani Ghamsari, N. Afshar, S. Lahuti. Mixed-phase TiO2 nanoparticles preparation using sol-gel method. *J. Alloys Compd.* **2009**, 478 (1–2), 586–589.
20. S. Myat, T. Htay, S. Nyein Khine, et al. XRD and SEM Analysis, and Semiconductor Type Determination of TiO2 for Dye-sensitized Solar Cell. ǁ *Int. Res. J. Adv. Eng. Sci.* **2019**, 4 (2), 103–107.
21. M.F. Rahman, Nasikhudin, A. Hidayat, M. Diantoro. The influence of TiO2 film thickness in Dye-Sensitized Solar Cells (DSSC) performance based on TiO2/Ag@TiO2-ZnO. *J. Phys. Conf. Ser.* **2020**, 1572 (1), 12079.
22. M. Khalid Hossain, M.F. Pervez, S. Tayyaba, et al. Efficiency enhancement of natural dye sensitized solar cell by optimizing electrode fabrication parameters. *Mater. Sci. Pol.* **2017**, 35 (4), 816–823.
23. F. Zulkifli, N. Ali, M.S.M. Yusof, et al. The effect of concentration of Lawsonia inermis as a corrosion inhibitor for aluminum alloy in seawater. *Adv. Phys. Chem.* **2017**, 2017, 1–12.
24. P.R. Kavitha Rani, A. Fernandez, A. George, et al. Synthesis, spectral characterization, molecular structure and pharmacological studies of N'-(1, 4-naphtho-quinone-2yl) isonicotinohydrazide. *Spectrochim. Acta. A. Mol. Biomol. Spectrosc.* **2015**, 135, 1156–1161.
25. C.A. Sesammal, P.R. Kavitha Rani, G. Sona. Synthesis, spectral characterization and molecular docking studies of lawsone derivatives as protein kinase inhibitors. *Asian J. Chem.* **2016**, 28 (12), 2737–2740.
26. K. Surana, M.G. Idris, B. Bhattacharya. Natural dye extraction from Syzygium Cumini and its potential photovoltaic application as economical sensitizer. *Appl. Nanosci.* **2020**, 10 (10), 3819–3825.
27. P.J. Singh Rana, P. Singh, P. Kar. Fluorescence alarming ON-OFF-ON switch derived from biocompatible carbon nanoparticle-hemoglobin-H2O2 interaction. *RSC Adv.* **2016**, 6 (74), 70660–70668.
28. M.J. García-Salinas, M.J. Ariza. Optimizing a simple natural dye production method for dye-sensitized solar cells: Examples for betalain (bougainvillea and beetroot extracts) and anthocyanin dyes. *Appl. Sci.* **2019**, 9 (12), 2515.
29. Y. Takeda, M.O. Fatope. New phenolic glucosides from lawsonia inermis. *J. Nat. Prod.* **1988**, 51 (4), 725–729.
30. N. Uddin, B.S. Siddiqui, S. Begum, et al. Bioactive flavonoids from the leaves of Lawsonia alba (Henna). *Phytochem. Lett.* **2011**, 4 (4), 454–458.
31. B.R. Mikhaeil, F.A. Badria, G.T. Maatooq, M.M.A. Amer. Antioxidant and immunomodulatory constituents of henna leaves. *Zeitschrift fur Naturforsch. - Sect. C J. Biosci.* **2004**, 59 (7–8), 468–476.
32. J.K. Ahmed. Effect of Chlorophyll and Anthocyanin on the Secondary Bonds of Poly Vinyl Chloride (PVC). *Int. J. Mater. Sci. Appl.* **2015**, 4 (2), 21.
33. K. V. Hemalatha, S.N. Karthick, C. Justin Raj, et al. Performance of Kerria japonica and Rosa chinensis flower dyes as sensitizers for dye-sensitized solar cells. *Spectrochim. Acta - Part A Mol. Biomol. Spectrosc.* **2012**, 96, 305–309.

34. N.E. Safie, N.A. Ludin, N.H. Hamid, et al. Electron transport studies of dye-sensitized solar cells based on natural sensitizer extracted from rengas (Gluta spp.) and mengkulang (Heritiera elata) wood. *BioResources* **2017**, 12 (4), 9227–9243.
35. A. Lim, N. Haji Manaf, K. Tennakoon, et al. Higher Performance of DSSC with Dyes from Cladophora sp. as Mixed Cosensitizer through Synergistic Effect. *J. Biophys.* **2015**, 2015, 1–8.
36. M. Shirkavand, M. Bavir, A. Fattah, H. Reza. The Construction and Comparison of Dye-Sensitized Solar Cells with Blackberry and N719 Dyes. *J. Optoelectron. Nanostructures* **2018**, 3 (1), 79–92.
37. J.M.K.W. Kumari, N. Sanjeevadharshini, M.A.K.L. Dissanayake, G.K.R. Senadeera, C.A. Thotawatthage. The effect of TiO2 photo anode film thickness on photovoltaic properties of dye-sensitized solar cells. *Ceylon J. Sci.* **2016**, 45 (1), 33.
38. F.M. Rajab. Effect of Solvent, Dye-Loading Time, and Dye Choice on the Performance of Dye-Sensitized Solar Cells. *J. Nanomater.* **2016**, 2016, 3703167.
39. M. Younas, K. Harrabi. Performance enhancement of dye-sensitized solar cells via co-sensitization of ruthenium (II) based N749 dye and organic sensitizer RK1. *Sol. Energy* **2020**, 203, 260–266.
40. H. Zhou, L. Wu, Y. Gao, T. Ma. Dye-sensitized solar cells using 20 natural dyes as sensitizers. *J. Photochem. Photobiol. A Chem.* **2011**, 219 (2–3), 188–194.
41. Z. He, J. Li, D. Wang, J. Wang, T. Zhang. Enhanced photovoltaic performance of TiO2 dye-sensitized solar cell based on one-dimensional composite photoanode. *Int. J. Electrochem. Sci.* **2017**, 12 (10), 8918–8928.
42. W. Maiaugree, S. Lowpa, M. Towannang, et al. A dye sensitized solar cell using natural counter electrode and natural dye derived from mangosteen peel waste. *Sci. Rep.* **2015**, 5, 15230.
43. P.S. Tamboli, M.B.R. Prasad, V.S. Kadam, et al. α-MoO3-C composite as counter electrode for quantum dot sensitized solar cells. *Sol. Energy Mater. Sol. Cells* **2017**, 161, 96–101.